Talanta 214 (2020) 120851

Contents lists available at ScienceDirect

Talanta

journal homepage: www.elsevier.com/locate/talanta

A nature-inspired colorimetric and fluorescent dual-modal biosensor for exosomes detection

Yaokun Xia[a,b,1], Tingting Chen[a,b,1], Guanyu Chen[a,b], Yunping Weng[a,b], Lupeng Zeng[a,b], Yijuan Liao[c], Wenqian Chen[a,b], Jianming Lan[a,b], Jing Zhang[c,**], Jinghua Chen[a,b,*]

[a] Department of Pharmaceutical Analysis, The School of Pharmacy, Fujian Medical University, Fuzhou, Fujian Province, 350122, PR China
[b] Fujian Key Laboratory of Drug Target Discovery and Structural and Functional Research, Fujian Medical University, Fuzhou, Fujian Province, 350122, PR China
[c] College of Life Sciences, Fujian Agriculture and Forestry University, Fuzhou, Fujian Province, 350002, PR China

ARTICLE INFO

Keywords:
Exosomes
Nature-inspired
DNA anchor
Colorimetric and fluorescent biosensor

ABSTRACT

As non-invasive biomarkers, exosomes are of great significance to diseases diagnosis. However, sensitive and accurate detection of exosomes still remains technical challenges. Herein, inspired by nature's "one-to-many" concept, we design a biosensor mimicking the cactus with numerous thorns to detect exosomes. The biosensor is composed of CD63 antibodies, resembling the roots of cactus, to capture exosomes, and the exosomes resemble the stems. Cholesterol-labeled DNA (DNA anchor) binding to streptavidin modified horseradish peroxidase (HRP) can insert into exosomes membrane, which seems the thorns. The readout signal is produced through HRP-catalyzed hydrogen peroxide (H_2O_2) mediated oxidation of 1,4-phenylenediamine (PPD) to form 2,5-diamino-NN′-bis-(*p*-aminophenyl)-1,4-benzoquinone di-imine (PPDox). The PPDox can quench fluorescence of fluorescein through inner filter effect (IFE), which provides fluorescent signal for exosomes detection. Based on this principle, the obtained exosomes solution is qualitatively and quantitatively analyzed by our biosensor, with the comparison to current standard methods by nanoparticle tracking analysis (NTA) and commercial enzyme-linked immunosorbent assay (ELISA) kit. The linear range is from 1.0×10^4 to 5.0×10^5 particles μL^{-1} with the limit of detection 3.40×10^3 particles μL^{-1} and 3.12×10^3 particles μL^{-1} for colorimetric and fluorescent assays, respectively. Meanwhile, our biosensor exhibits good selectivity, and can eliminate the interference from proteins. This dual-modal biosensor shows favorable performance towards analytical application in clinic samples, pushing one step further towards practical clinical use.

1. Introduction

Exosomes are membrane-bound extracellular phospholipid vesicles that are actively secreted by almost all types of cells, and can enter different body fluids, such as blood, cerebrospinal fluid (CSF), urine and breast milk [1,2]. Growing evidences have demonstrated that exosomes are acted as promising mediators for regulating long-range intercellular communication in the body by transferring protein and nucleic acid molecules, involving in physiological and pathological processes [3–7]. Currently, more and more researches report that exosomes are potential to become non-invasive biomarker for certain diseases in liquid biopsy field because of their increasing concentration in systemic circulation, especially for autoimmune disease and cancer [8–10]. However, as relatively new target for bioassays, exosomes possess unique physical and biological traits. For example, the size of exosomes is larger than proteins but much smaller than cells. In addition, there are complex components on exosomes surface. Above properties make them difficult to be analyzed [11]. Thus, active researches are underway to surmount these challenges and to optimize exosomes analysis platform.

Currently, according to the minimal information for studies of extracellular vesicles 2018 (MISEV 2018), the accepted accredited methods for exosomes detection including nanoparticles tracking analysis (NTA), tunable resistive pulse sensing (RPS), flow cytometry, cryo-EM, a platform combining surface plasmon resonance (SPR) with AFM, or by other techniques with similar capabilities have been developed [12]. However, the following three aspects of drawbacks limit their application scope. First, many of methods require state-of-the-art instruments. Secondly, the selectivity for some specific exosomes is

* Corresponding author. Department of Pharmaceutical Analysis, The School of Pharmacy, Fujian Medical University, Fuzhou, Fujian Province, 350122, PR China.
** Corresponding author.
E-mail addresses: 1601225385@qq.com (J. Zhang), cjh_huaxue@126.com (J. Chen).
[1] These authors make equal contribution to the paper.

https://doi.org/10.1016/j.talanta.2020.120851
Received 28 October 2019; Received in revised form 13 February 2020; Accepted 15 February 2020
Available online 19 February 2020

deficient. Thirdly, the accuracy is often influenced by unreliable nanoparticle counting, which is from large proteins aggregate and lipoprotein particles, and even some exosomes less than a certain size being omitted [13]. Fortunately, with the in-depth research, different approaches with recognition element were reported, including colorimetric methods [14,15], fluorescent assays [16–28], surface plasmon resonance spectroscopy [29,30], microfluidic technologies [31,32], surface enhanced Raman scattering (SERS) [33–37], electrogenerated chemiluminescence (ECL) methods [38], and electrochemical strategies [39–43], etc. Among them, the optical strategies have drawn much attention. For instance, the colorimetric method is simple, rapid and visualized, which is potential for developing portable Point of Care testing (POCT) device for exosomes analysis. As for fluorescent strategy, it possesses high sensitivity, fast response time as well as practical feasibility in biological system. Therefore, by integrating colorimetry-based detection and fluorescence-based detection into a dual-modal biosensor, the advantages of two types are combined for exosomes detection.

Besides, because of the trace concentration of disease related exosomes in real bio-samples, the sensitivity is vital for the performance of method. Although several attempts have been reported to improve the sensitivity, the practicability is hampered by the tedious DNA sequences design [42], complicated nanomaterials synthesis and sophisticated interface modification [20,44], etc. Fortunately, the recent emergence of some nature-inspired systems for detecting various targets impels us to get inspiration in nature [45–47]. As observed in numerous organisms, nature has offered a large amount of concise engineering designs, such as cactus. For instance, there are a large number of thorns on surface of one bulb of cactus. Inspired by cactus, we search for a versatile strategy to engineer the surface of exosomes by integrating this biological system design notion into our biosensor, exhibiting that it is possible to develop a detection platform for analyzing exosomes sensitively. Interestingly, because of the special nanostructure of exosomes, they can be modified by different mechanisms that is similar to other nanomaterials [48–52], giving them more functions. According to previous reports, physical interactions (hydrophobic interaction) [53], genetic manipulations [54], and construction of specific affinity sites are developed to modify the lipid membrane [1]. It is worth noting that modification exosomes surface by hydrophobic interaction via a lipid moiety, such as monoacyl lipid (C18), cholesterol, and diacyl lipid (DSPE) is an efficient strategy compared with other strategies, because of its simplicity, low toxicity, fastness, high speed, and the low number of exosomes surface proteins being affected [55]. Consequently, using this technique is a powerful way to make exosomes membrane gain large number of desirable components and new functions.

In this work, mimicking the structural characteristics of the cactus, a CD63 antibody-based biosensor is designed for exosomes analysis (Scheme 1A). Considering the amount of CD63 in different exosomes is discrepant [56], it is chosen as targeted protein in this work and acted as a model to validate the feasibility of our biosensor for exosomes detection. The biotinylated CD63 antibody is employed to act as recognition element and captures exosomes. The DNA anchors are able to spontaneously insert into the hydrophobic interior of lipid membranes and the DNA orientated at the aqueous phase. As a result, a large number of DNA anchors are enriched on the surfaces of exosomes, and the biotin modified on the other end of DNA anchor can bind with substantial streptavidin tagged HRP that acts as signal transducer. Subsequently, the HRP catalyzes colorless PPD/H_2O_2 system, producing brown oxidized product (PPDox) (Scheme 1B). The absorbance of PPDox is directly proportional to the concentration of exosomes. Moreover, adding fluorescein into the PPDox solution, the fluorescence intensity is quenched by PPDox through IFE [57], which produces a fluorescent readout signal. Other than previous works [58,59], the fluorescence quenching effect of IFE is not related to the distance between fluorescence substrate and quencher, so preparation of linker element is not essential, which simplifies the detection steps [60]. For instance, Chen's group and Wang's group developed a relatively simple and facile dual-modal biosensor based IFE for targets detection [61,62]. On the basis of above facts, it is urgent and possible to develop a colorimetric and fluorescent dual-modal biosensor for exosomes detection. The as-design dual-modal biosensor can also be applied to other types of exosomes markers analysis as well as further research on the disease-related biomedical processes.

2. Experimental methods

2.1. Reagent and apparatus

All oligonucleotides were synthesized by TaKaRa Biothchnology Co., Ltd. (Dalian, China), and the sequences were illustrated in Table S1. PPD was purchased from Tokyo Chemical Industries (TCI, Japan). Avidin modified HRP was purchased from Beijing Biosynthesis Biotechnology Co., Ltd. The fluorescein sodium salt and dulbecco's phosphate buffered saline (DPBS) were purchased from Sigma-Aldrich. Biotin modified CD63 antibody was purchased from Abcam. The streptavidin modified 96-well plates were obtained from Thermo Fisher Scientific. All cell lines were obtained from China Center for Type Culture Collection in Shanghai. Roswell Park Memorial Institute (RPMI), Dulbecco's Modified Eagle medium (DMEM), and phosphate buffer saline (PBS) were purchased from Hyclone. Mammary Epithelial Cell Growth Medium (MEGM) BulletKit was obtained from Lonza. Ultrapure water (18.2 MΩ) was used in all aqueous solution. The buffers utilized in this assay were as follows: (1) DPBS buffer contains 25 mmol L^{-1} glucose; (2) wash buffer was purchased from Thermo Fisher Scientific; (3) phosphate buffer (PB) contained 20 mmol L^{-1} sodium dihydrogen phosphate and 20 mmol L^{-1} disodium hydrogen phosphate (pH 7.0). The ultracentrifuge was Beckman optima XPN-100 (U.S.A.). The absorption and fluorescence spectra were obtained from Cary-60 spectrophotometer (Agilent Technologies) and Cary Eclipse fluorescence spectrofluorometer (Agilent Technologies), respectively.

2.2. Isolation of exosomes

Human breast cancer cells MDA-MB-231 and MCF-7 were cultured in RPMI-1640 and DMEM, respectively, both containing 10% (v/v) fetal bovine serum (FBS), 1% penicillin-streptomycin (v/v). Human breast normal cells MCF-10 A were cultured in MEGM containing cholera toxin. All above cells were maintained in a humidified atmosphere of 5% CO_2 at 37 °C. The MDA-MB-231 and MCF-7 cells were cultured in culture medium containing 10% FBS (exosomes depleted) for 48 h before ultracentrifugation. To collect exosomes, the cell culture supernatant was treated as follows: it was centrifuged at 300 *g* for 10 min, 2,000 *g* for 20 min and 11,000 *g* for 45 min at 4 °C to remove intact cells, cells debris and protein, respectively. Finally, the supernatant was ultracentrifugation at 110,000 *g* for 70 min. After removing the supernatant, the exosomes pellet was resuspended in cold sterile PBS, and was ultracentrifugated again at 110,000 *g* for 70 min. The sediment exosomes were collected, and resuspended in sterile PBS for further application.

2.3. The modification of cell membrane and exosomes membrane with DNA anchor

The modification of cell membrane with DNA anchor followed adapted procedures [63]. 500 nmol L^{-1} fluorescein conjugated DNA anchor was incubated with 5×10^5 cells mL^{-1} in 200 μL DPBS buffer at 4 °C for 60 min. Subsequently, the cells were centrifuged at 1200 rpm for 5 min to remove the uncombined DNA anchors. The confocal microscope images were obtained by a Zeiss LSM880.

As for exosomes membrane modification, the 2.5 μL 10 mg mL^{-1} streptavidin coated MBs and 0.5 μL CD63 biotinylated antibody were incubated in 97 μL PBS for 30 min at room temperature. Next, the

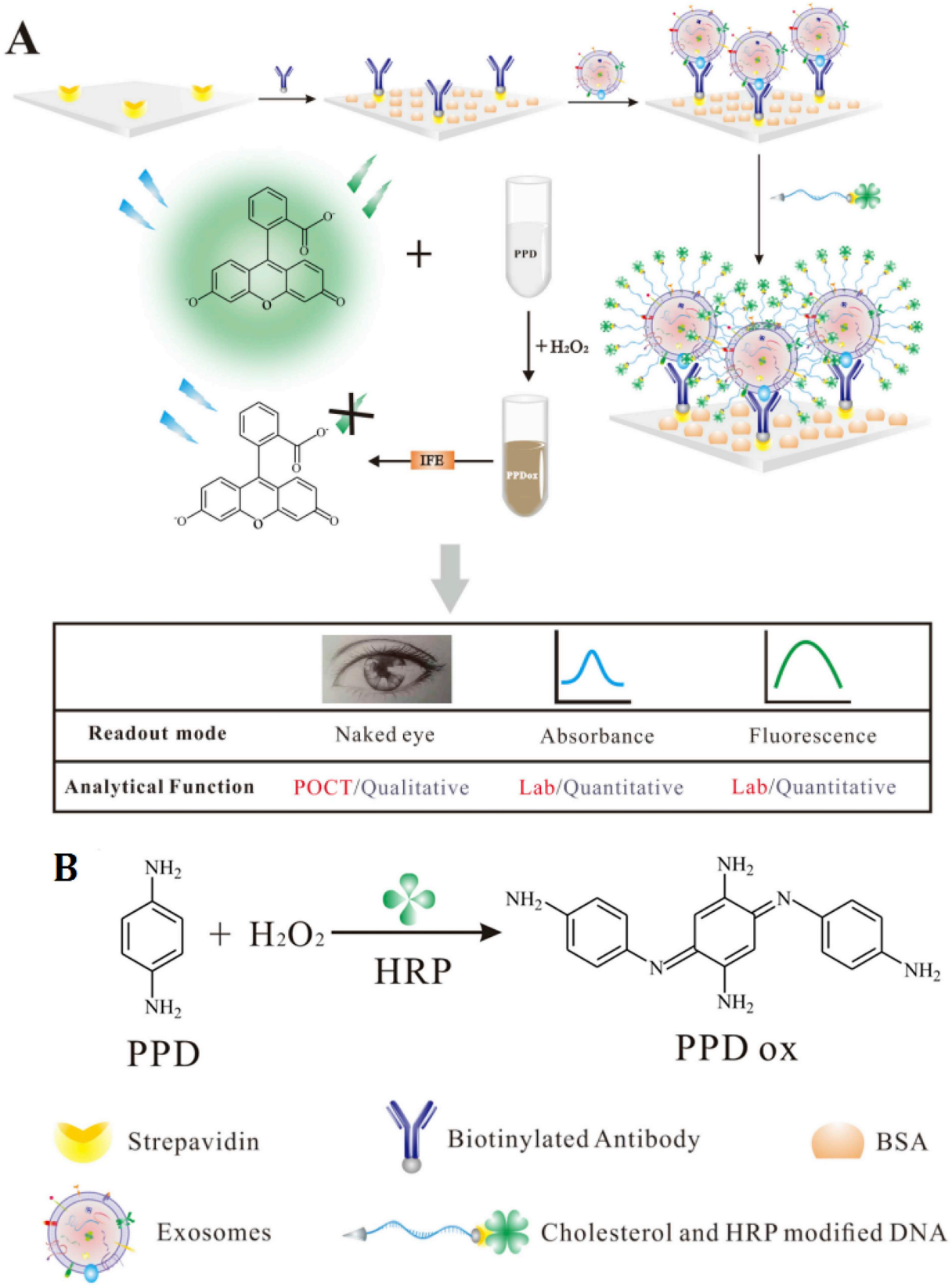

Scheme 1. (A) Working principle of the proposed method for exosomes detection. (B) Schematic representation of HRP-catalyzed oxidation of PPD into PPDox by H_2O_2.

exosomes solution were mixed with above MBs, and reacted for 60 min at room temperature. Then, the supernatant was removed, and the MBs were washed by three times. After that, the MBs were dispersed in DPBS buffer containing 1 μmol L^{-1} fluorescein conjugated DNA anchor, and reacted for 120 min at 4 °C. Subsequently, the supernatant was removed. The prepared MBs were imaged by a Zeiss LSM880

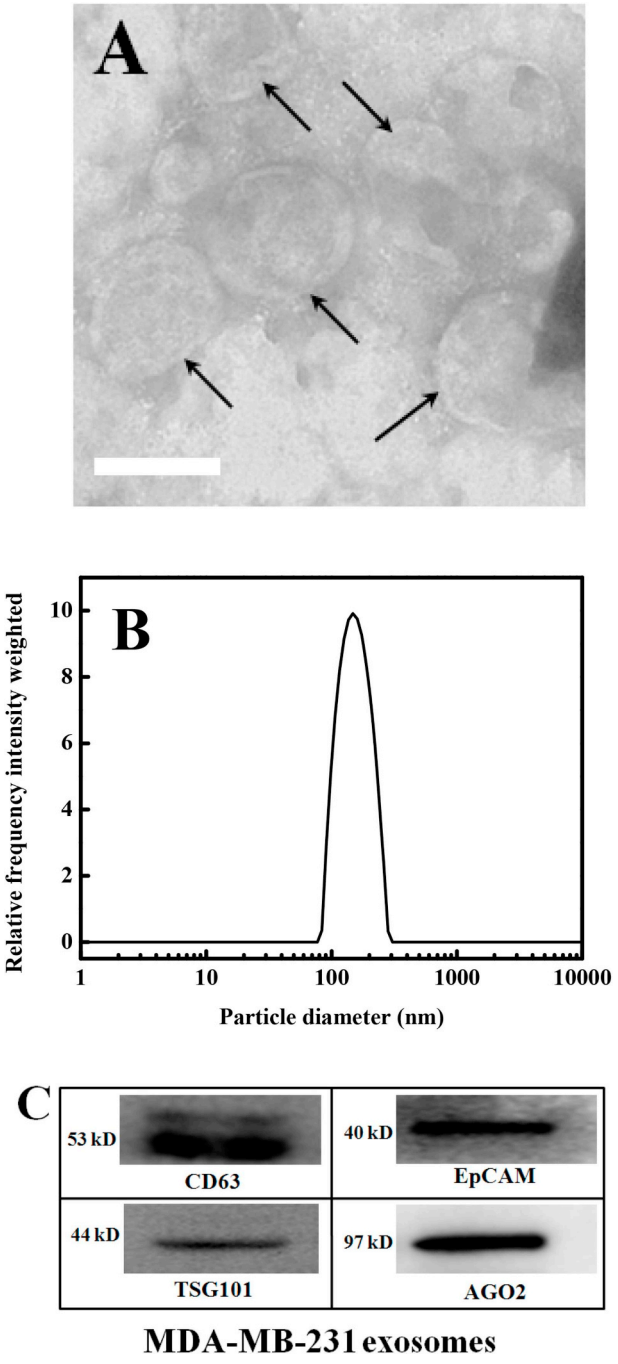

Fig. 1. (A) TEM images of MDA-MB-231 exosomes, (B) Size and size distribution of the MDA-MB-231 exosomes, (C) WB images for different types of proteins in MDA-MB-231 exosomes. The scale bar represents 100 nm.

confocal fluorescent microscope.

2.4. The feasibility of detection of exosomes by this biosensor

An established protocol for 96-well plate modification follows the modified instructions. Before being used, each well was washed three times with wash buffer. 100 μL 10 μg mL^{-1} biotinylated CD63 antibody (anti-CD63) was added and incubated for 1 h with shaking and used to capture exosomes followed by three washes with wash buffer. The antibody-coupled 96-well plate was blocked with 200 μL block buffer containing 5 μg streptavidin for 60 min, and washed three times. After washing, the exosomes of a serial dilution were added to each well and placed on the plate for 2 h at 4 °C. The wells were repeatedly washed three times, following which the DNA anchor and HRP (DNA anchor-HRP) were added to each well and incubated for 80 min at 4 °C. After removal and washing steps, 1 mmol L^{-1} PPD, 1 mmol L^{-1} H_2O_2, and PB were added until the volume reached 100 μL. The absorption spectra of the mixture solution were measured after reaction at dark for 20 min. In addition, the fluorescence spectra were recorded immediately after the 30 μmol L^{-1} fluorescein sodium salt being added to the mixture solution.

2.5. Immunoaffinity-based exosomes detection

Colorimetric strategy: exosomes of different concentration (0, 0.1, 0.5, 1.0, 1.5, 2.5, 3.0, 4.0, 5.0 × 10^5 particles μL^{-1}) were added to CD 63 antibody coated 96-well plate. Other procedures followed the experimental steps described in Section 2.4. Fluorescent strategy: 30 μmol L^{-1} fluorescein was added into above plate, and other procedures followed the experimental steps described in Section 2.4.

3. Results and discussion

3.1. Experimental principle of the dual-modal biosensor

As illustrated in Scheme 1A, this approach includes following three parts: (1) immunoaffinity capture of exosomes; (2) DNA anchor-HRP inserting into exosomes membrane for signal conversion; (3) catalyzing PPD/H_2O_2 system to producing PPDox, and quenching fluorescence of fluorescein, resulting in change of colorimetric and fluorescent signals, respectively. Herein, the biotinylated CD63 antibody is immobilized onto the streptavidin-modified 96-well plates for capturing exosomes. Then, the HRP connected DNA anchor is incorporated into the bilayer of captured exosomes through hydrophobic reaction between cholesterol and exosomes membrane, which results in abundant signal conversion units being integrated into exosomes. In the presence of PPD and H_2O_2, the HRP catalyzes H_2O_2 to oxide PPD producing PPDox, allowing this system colour changed from colorless to brown with absorption maximum at λ = 500 nm, which is able to be observed by naked eyes and measured by UV–vis spectroscopy. Moreover, adding fluorescein sodium salt into the final solution, the fluorescence is quenched by PPDox based on IFE. The absorbance and fluorescence intensity both are correlated with the concentration of exosomes, enabling the qualitative and quantitative dual-modal detection of exosomes.

3.2. The characterization of exosomes

The exosomes secreted by MDA-MB-231 cells are collected from the cell culture supernatant using ultracentrifugation for following analysis. The abundance of acquired exosomes is quantified by standard curve that obtained from commercial immunoassays (ExoELISA-ULTRA Complete Kit). As shown in Fig. S1, the corresponding standard curve is described as A = 0.62779 N + 0.11816, r = 0.9951 (N represents the number of exosomes). Based on above standard curve, the exosomes abundance is about 3.0 × 10^8 particles μL^{-1}. The concentration is close to that detected by NTA (Fig. S2). On the basis of International Society for Extracellular Vesicles (ISEV) guidelines [12], the morphology of acquired exosomes is characterized first. TEM results exhibit that the all obtained exosomes show mean diameter about 100 nm and saucer-like structure (Fig. 1A). Next, the size distribution of the exosomes is measured by dynamic light scattering (DLS). As shown in Fig. 1B, the average diameter for MDA-MB-231 exosomes is 148 nm. Noteworthily, the difference of diameter from TEM and DLS results is ascribed to the fact that the exosomes are shrunk or changed size during the preparation process for TEM, which is one of reasons for causing the smaller size for exosomes utilizing TEM [64]. The other reason is that DLS results show hydrodynamic diameter, which leads to large nanoparticles

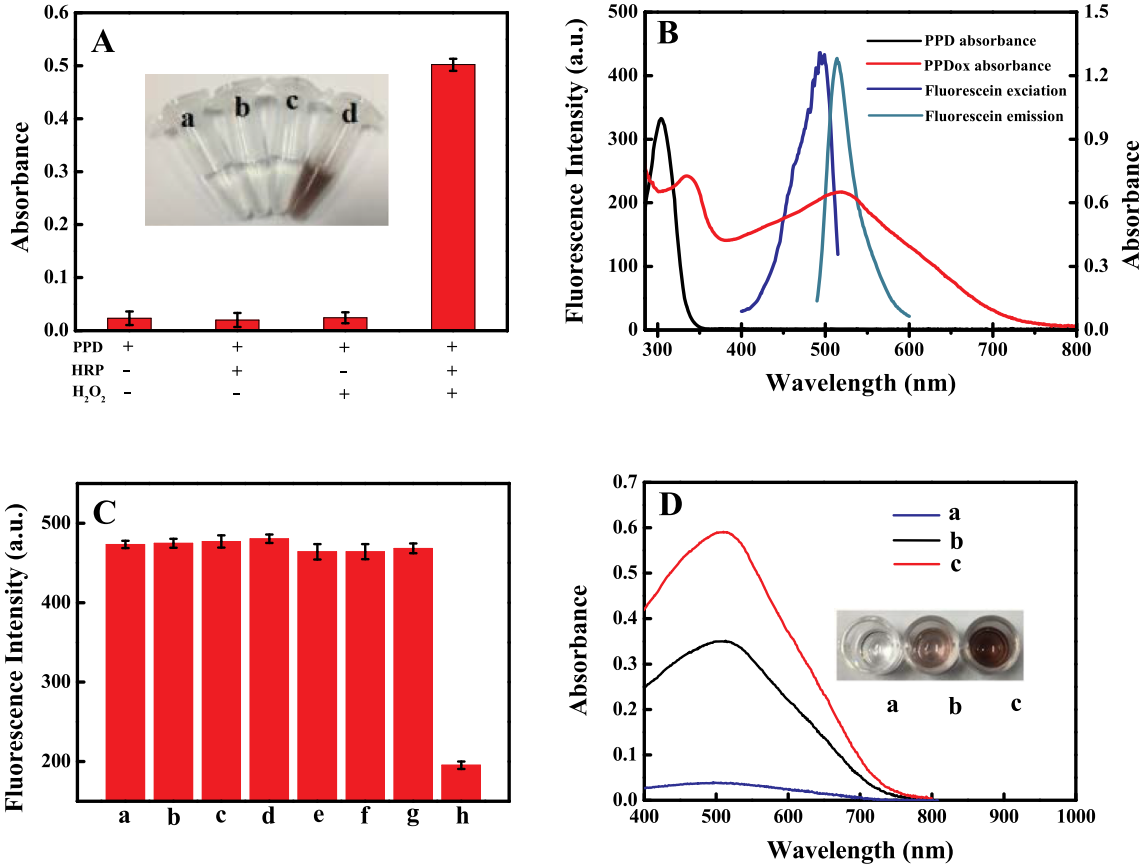

Fig. 2. (A) Absorbance of PPD, PPD + HRP, PPD + H_2O_2 and PPD + H_2O_2 + HRP in phosphate buffer at pH 7.0. Inset: the corresponding digital images. (B) Absorption spectra of PPD (black) and PPDox (red). Fluorescence excitation (blue) and emission (green) spectra of fluorescein. (C) Fluorescence intensities of fluorescein (a), fluorescein + H_2O_2 (b), fluorescein + PPD (c), fluorescein + HRP (d), fluorescein + HRP + H_2O_2 (e), fluorescein + HRP + PPD (f), fluorescein + PPD + H_2O_2 (g), fluorescein + HRP + H_2O_2 + PPD (h). (D) UV–vis absorption spectra of the reaction system in the absence (curve a) and presence of different concentration exosomes (curve b and c). Inset: the corresponding digital images. (For interpretation of the references to color in this figure legend, the reader is referred to the Web version of this article.)

contributing more strongly than the small nanoparticles for light scattering, leading to size shift in the size distribution values [56]. Subsequently, different categories of proteins including CD63 and EpCAM (transmembrane or lipid-bound extracellular protein), TSG101 (cytosolic protein), and Argonaute 2 (AgO2, intracellular protein) were validated by Western blot (WB). From Fig. 1C, the obvious bands demonstrate that CD63, EpCAM, TSG101, and AgO_2 are present in the MDA-MB-231 cells secreted exosomes.

3.3. The feasibility of this biosensor

3.3.1. HRP catalyzing H_2O_2-mediated oxidation of PPD

In Fig. 2A, the solution is colorless when only PPD is present (photo a), and the UV–vis absorbance is weak at 500 nm. Similarly, when add either HRP or H_2O_2 into the PPD, the solution colour and absorbance are not changed (photo b and photo c). On the contrary, when H_2O_2, HRP and PPD are present in a system, the colour (photo d) and absorbance of solution exhibit an obvious change, where HRP can catalyze H_2O_2-PPD system, oxidizing colorless PPD into the brown PPDox. The experimental procedures are described in S1 (Supporting Information).

3.3.2. Fluorescence quenching of fluorescein by PPDox

The maximum excitation and emission wavelengths of fluorescein are overlapped by the absorption spectrum of PPDox (Fig. 2B), which results in the fluorescence quenching through IFE [57]. In addition, the fluorescence intensities of fluorescein in different systems are explored. As shown in Fig. 2C, compared with fluorescein itself (column a), the fluorescence intensities are almost not changed after individual addition of H_2O_2 (column b), PPD (column c) or HRP (column d) into fluorescein solution. Similarly, the fluorescence intensity of fluorescein is not decreased by addition of the mixture solution of HRP/H_2O_2 (column e), HRP/PPD (column f), or PPD/H_2O_2 (column g), which is ascribed to none of PPDox formation in these solutions. When PPD, H_2O_2 and HRP all are added into fluorescein solution simultaneously, an obvious fluorescence quenching is occurred (column h), because of formation of PPDox and exhibiting significant absorption peak at 500 nm. The experimental procedures are described in S2 (Supporting Information).

3.3.3. The modification of lipid bilayer with DNA anchor

Firstly, we employ MDA-MB-231 cell as a model to validate the feasibility of DNA anchor being able to insert into lipid bilayer, because both cell membrane and exosomes membrane are lipid bilayers. As shown in Fig. S3, after incubating fluorescein labeled DNA anchor with MDA-MB-231 cells and removing unbound anchors, the cell membrane can be clearly observed under laser confocal microscopy, which demonstrates that lipid bilayer is efficiently modified by DNA anchor. The results are similar to the previous report [63]. Meanwhile, in order to intuitively exhibit the DNA anchor inserting into the lipid bilayer of the exosomes, we introduce magnetic beads technology, and take images by laser confocal microscopy. The experimental mechanism is displayed in Scheme S1. Interestingly, the bright green fluorescence of the magnetic beads is observed clearly

(Fig. S4), which evidences that the DNA anchor can also insert into the exosomes surface.

3.3.4. Detection of exosomes by this biosensor

As shown in Fig. 2D, when exosomes are absence, the solution is colourless (photo a), and the absorbance at 500 nm is neglectable (curve a). However, in presence of exosomes, the colour of solution shows significant change (photo b), and absorbance is increased obviously (curve b). Importantly, the colour and absorbance of solution are dependent on the concentration of exosomes (photo c and curve c). Meanwhile, as shown in Fig. S5, the fluorescence intensities of fluorescein in presence of exosomes (curve a and b) are significantly lower than that in absence of exosomes (curve c), which is ascribed to the generated PPDox quenching the fluorescence of fluorescein. Thus, above results indicate that this proposed biosensor is feasible for exosomes analysis.

3.4. Optimization of the experimental parameters

To optimize the assay performance, we first utilize exosomes that is purified by ultracentrifugation as targets to optimize the experimental conditions, including the incubation time between antibody and exosomes, DNA anchor concentration, anchor time, colorimetric pH value, fluorescein concentration, and pH value for fluorescence intensity. The experimental procedures are described in S3 (Supporting Information). As shown in Fig. S6A, with the increase of incubation time between exosomes and CD63 antibody, the ΔA value is also increased (the ΔA represents A-A_0, A and A_0 represent the absorbance at 500 nm in the presence and absence of exosomes, respectively). The ΔA reaches maximum when incubation time is 120 min, so it was chosen for the optimal incubation time between exosomes and CD63 antibody. The DNA anchor concentration has a significant effect on the catalysis. In Fig. S6B, the ΔA increased obviously when the DNA anchor concentration is increased. Nevertheless, when the DNA anchor concentration is higher than 1000 nmol L^{-1}, the absorbance reaches a plateau, suggesting the optimal concentration of DNA is 1000 nmol L^{-1}. Moreover, the reaction between DNA anchor and exosomes lipid bilayer membrane relies on the incubation time. Under the optimum concentration of DNA, 80 min is chosen as the optimal incubation time (Fig. S6C). The pH value can influence the detection performance. In Fig. S6D, the ΔA increases to a maximum at pH 7.0, and then decreases, suggesting that a physiological condition is suitable. As for the fluorescence analysis, the concentration of fluorescein is important. In Fig. S6E, the change of fluorescence intensity (ΔF is defined as F_0–F, F_0 and F mean the fluorescence intensity at 520 nm in the absence and presence of exosomes, respectively) exhibits a gradual increase at first, while the fluorescence intensity is dramatically decreased at high concentration, which is ascribed to the inherent self-absorption effect [57]. Therefore, we chose 30 μmol L^{-1} as the optimal concentration for fluorescein. At the same time, we find that the fluorescence intensity is weak at low pH values, but the maximal intensity is observable in neutral and alkaline solution (Fig. S6F). Consequently, the fluorescence detection is conducted under the neutral condition. Similarly, the neutral solution is beneficial to the HRP activity and colorimetric assay.

3.5. The performance of this biosensor

Under above optimum conditions, the proposed colorimetric biosensor with fluorescent readout as complementary signal is performed for exosomes detection. The UV–vis absorbance at 500 nm increases as the concentrations of exosomes increasing from 1.0×10^4 particles μL^{-1} to 5.0×10^5 particles μL^{-1} (Fig. 3A). The colour change of solution is obvious with the addition of different concentrations exosomes (Fig. 3A, inset). The absorbance intensity is linearly dependent on the exosomes concentration (Fig. 3B). The corresponding work curve could be expressed as $\Delta A = 0.10955C$ (10^5 particles μL^{-1})-0.00323 ($r = 0.9946$). The limit of detection (LOD) based on 3σ method is 3.40×10^3 particles μL^{-1}. Simultaneously, a complementary fluorescent detection is also performed. The fluorescein is added into above reaction solution at optimal concentration. As shown in Fig. 3C, the fluorescence intensity is decreased gradually with the increasing of exosomes concentration. From Fig. 3D, the calibration plot also exhibits good linear relationship between ΔF and the exosomes concentration from 1.0×10^4 particles μL^{-1} to 5.0×10^5 particles μL^{-1} with a lower LOD 3.12×10^3 particles μL^{-1}. Besides, the correlation equation is $\Delta F = 62.611C$ (10^5 particles μL^{-1})-1.1898 ($r = 0.9926$). The high sensitivity of this biosensor can be ascribed to the following reasons: (1) The high affinity of antibody improves the capture efficiency at low exosomes concentration. (2) Cholesterol-based hydrophobic reaction allows many DNA anchors spontaneous to insert into the exosomes membrane, providing a signal amplification avenue. Because of the high sensitivity, this biosensor can detect exosomes in cell supernatant directly. However, to avoid the interferences from dead cells, cells debris and large vesicles, some simple centrifugation steps are still needed to remove above impurity. As shown in Fig. S7A, with increase of exosomes amount, the UV–vis absorbance is also increased. There is good linear relationship between exosomes concentration and absorbance (Fig. S7B). Meanwhile, the fluorescence intensity is also gradually decreased when detecting exosomes in cell supernatant (Fig. S7C), and a dose-response curve is also acquired (Fig. S7D), which indicates our biosensor can detect exosomes in cell supernatant directly. In addition, a comparison of this biosensor and currently available methods for exosomes is displayed in Table S2. Compared with a number of methods, the LOD of our biosensor is superior [14,15,23,27]. Moreover, the LOD of some other strategies is comparable of this method, but complex DNA sequences design [13,19] and synthesis of nanomaterials like gold nanorods [33], lipsomes and upconversion nanoparticles [17,20] are required, which is sophisticated and time-consuming for exosomes detection. Although some reports exhibit higher sensitivity than proposed biosensor, the unstable electrochemical strategies often influence the accuracy of detection [39–42,65]. Besides, the tedious probe modification is labour-consuming [28,34,66], which may decrease the detection efficiency. Furthermore, the detection range of NTA is from 10^3 to 10^6 particles μL^{-1}, but the high cost, poor selectivity and readily interfered large protein particles hinder its application field. To further improve the sensitivity and reduce detection time of our biosensor, we plan to select recognition elements with higher affinity, and develop a label-free and wash-free strategy for exosomes detection in the future.

The selectivity of this biosensor toward exosomes and other proteins is studied. As shown in Fig. S8, the human serum albumin (HSA), albumin from bovine serum (BSA), and immunoglobulin (IgG) are tested under the optimized conditions. The change of UV–vis absorbance and fluorescence intensity of these proteins are almost neglectable compared with those of exosomes, which is ascribed to the specificity of antibody for CD63 and the hydrophobic reaction between DNA anchor and exosomes membrane. Next, this biosensor is employed to detect different cells-derived exosomes. Before the detection assay, the morphology, size and exosomal proteins of MCF-7 cells-originated exosomes and MCF-10 A cells-originated exosomes are characterized by TEM, DLS and WB, respectively (Fig. 4A and B). As displayed in Fig. 4C, when three different cells-originated exosomes (including MDA-MB-231 exosomes, MCF-7 exosomes and MCF-10 A exosomes) are present, the signals are changed significantly based accordingly on the origin of exosomes. It is worth noting that the tendency of the changes in signal intensities is consistent with that obtained from Western blot (Fig. S9), which demonstrates that our method is able to distinguish the amount of CD63 protein on different exosomes. As far as we know, CD63 protein not only exists in tumorigenic exosomes (MDA-MB-231 cells-derived exosomes and MCF-7 cells-derived exosomes), but it also exists in non-tumorigenic exosomes (MCF-10 A cells-derived exosomes).

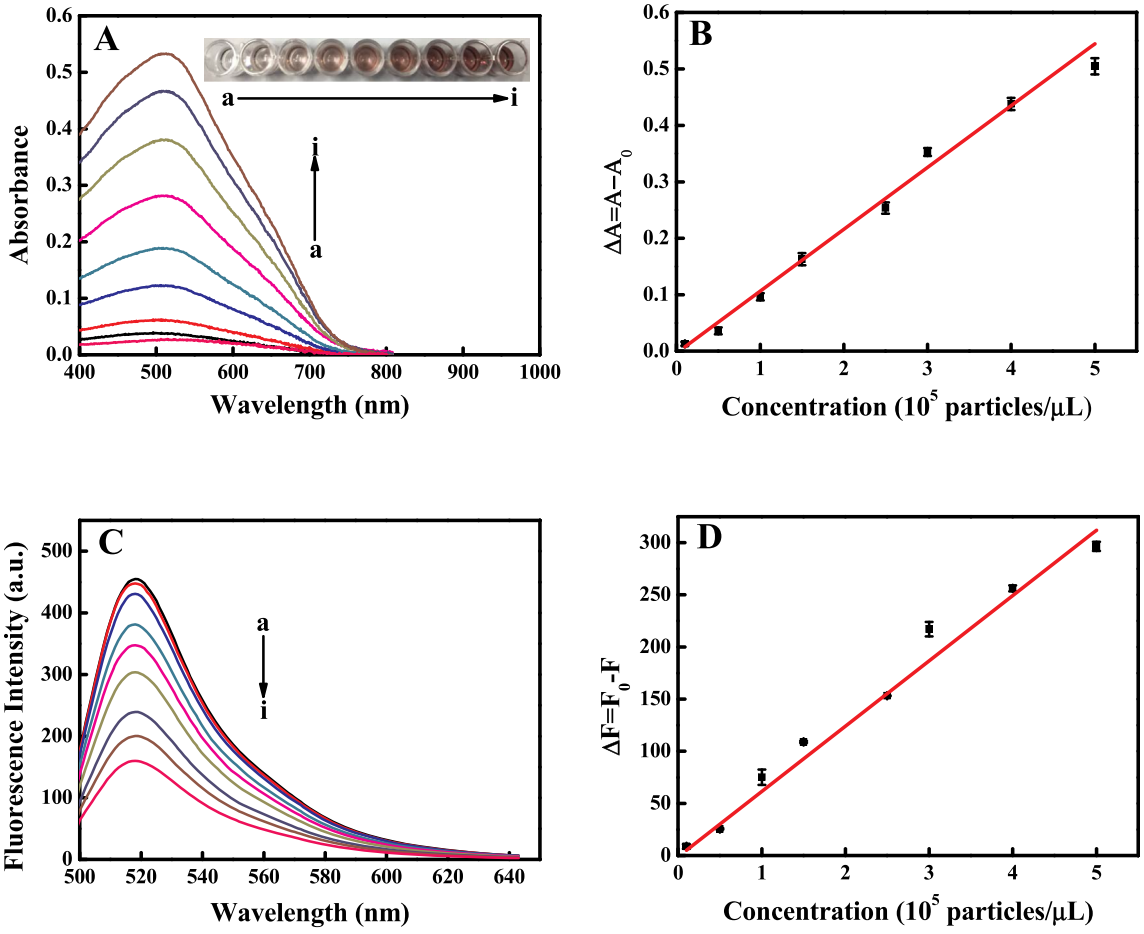

Fig. 3. (A) UV–vis absorbance response for different concentrations of exosomes, (a) 0, (b) 0.1, (c) 0.5, (d) 1.0, (e) 1.5, (f) 2.5, (g) 3.0, (h) 4.0, (i) 5.0 × 10^5 particles/μL. Inset: the corresponding digital images. (B) Linear relationship of ΔA versus exosomes concentration. (C) Fluorescence spectra of the proposed assay in the presence of different concentrations of exosomes, (a) 0, (b) 0.1, (c) 0.5, (d) 1.0, (e) 1.5, (f) 2.5, (g) 3.0, (h) 4.0, (i) 5.0 × 10^5 particles/μL. (D) Linear relationship of ΔF versus exosomes concentration.

However, the amount of CD63 proteins in non-tumorigenic exosomes is less than tumorigenic exosomes. Additionally, the latest standard from the International Society for Extracellular Vesicles (ISEV) demonstrates that there is no gold standard to distinguish the specificity of exosomes [12]. Consequently, we chose CD63 protein as a model to study the feasibility of our biosensor for universal exosomes detection method. We believe that with the discovery of more and more specific markers on exosomes, adapting this proposed method with specific capture element may further improve the capacity of distinguishing different exosomes. Therefore, we envision that our strategy provides a potential research foundation for a universal exosomes detection method.

3.6. Biological sample applications

To validate the practical application of our biosensor, we first add five levels of exosomes ranging from 0.5 × 10^5 to 4.0 × 10^5 particles μL^{-1} into 1% diluted exosomes depleted FBS to simulate a biological sample. Every sample is measured in triplicate. The experimental procedures are shown in S4 (Supporting Information). As shown in Table 1, the recovery rates ranged from 96.0% to 110.33% and from 84.0% to 114.0% for colorimetry and fluorescence detection, respectively. The P-value by *t*-test is 0.43 that is larger than 5%, suggesting there is no significant difference between the detection results from two different signals (Fig. S10). The relative standard deviation (RSD) is between 0.91% and 7.38% for colorimetric method as well as between 0.90% and 4.33% for fluorescent method, which indicates that our biosensor exhibits favorable stability (Table 1). In a word, above results indicate that our strategy detection exosomes in real sample is feasible.

To further validate the applicability in real biological samples, this biosensor is employed to analyze clinical serum samples. The experimental procedures are shown in S5 (Supporting Information). The serum samples were obtained from the Fuzhou Second Hospital. Written informed consents were obtained from all participants. All experiments were performed in accordance with relevant guidelines and were approved by the Ethics Committee of Fuzhou Second Hospital (Ethical certification No. 20180027). Ten clinic serum samples from breast cancer patients and healthy donors are analyzed by our method. Meanwhile, as a control to investigate the accuracy of our proposed method, we utilize commercial immunoassays to measure the amount of the obtained exosomes. Fig. 5A shows that the results obtained from this biosensor are comparable with those that acquired from commercial immunoassays. It is worth note that the concentrations of exosomes from breast cancer patients and healthy donors are significantly different in statistics ($P < 0.05$) (Fig. 5B), which is ascribed to the higher expression of CD63 in breast cancer patients serum derived exosomes than healthy donors serum derived exosomes [67]. However, it is a

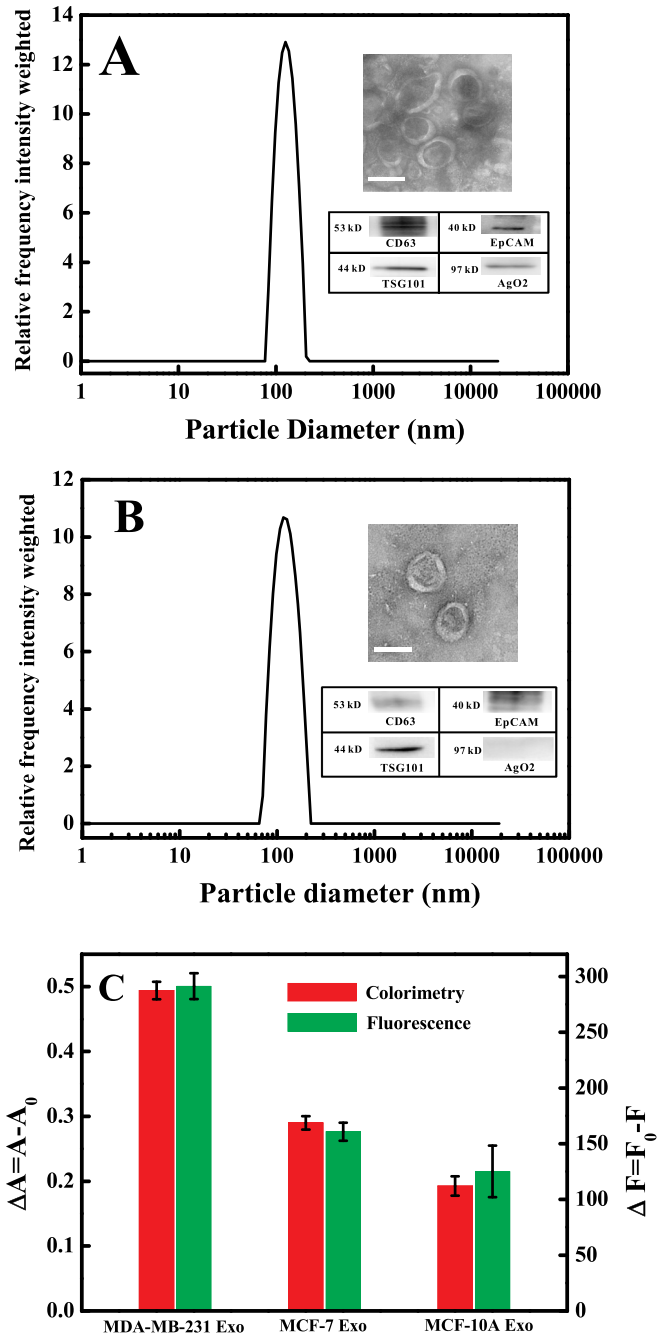

Fig. 4. (A) The size and size distribution of the MCF-7 exosomes, inset: the TEM image of MCF-7 exosomes (top panel), the WB images of different types of proteins in MCF-7 exosomes (down panel). (B) The size and size distribution of the MCF-10 A exosomes, inset: the TEM image of MCF-10 A exosomes (top panel), the WB images of different types of proteins in MCF-7 exosomes (down panel). The scale bars represent 100 nm. (C) Histogram of the ΔA and ΔF for different cells derived exosomes.

difficulty and research focus to classify, specific isolate and detect cancer cells derived exosomes in the circulation to date. In order to improve diagnostic accuracy, various methods including immunoaffinity assay [43], aptamer technology [24], microfluidic technology [68], etc., were developed. Nevertheless, there is still barrier for specific isolation of exosomes because specific markers for cancer cells derived exosomes are still unknown [69]. In this work, although the CD63 protein is not cancer-type specific, its aberrant expression on exosomes is related to malignancy to a certain extent. We envision that with the discovery of specific proteins on exosomes surface in the future, it is possible to detect cancer related exosomes simply by changing the recognition element of our biosensor, thus improving the ability of distinguishing different exosomes. While more clinic samples need to be tested in future work to further validate the feasibility for breast cancer diagnosis and monitoring, this assay exhibits potential to provide a reliable assay for quantification of exosomes.

4. Conclusion

In conclusion, we designed a cactus-inspired dual-modal biosensor for qualitative and quantitative detection of exosomes. The proposed method is composed of immunoaffinity isolation, lipid membrane modification, and signal readout based on the change of UV–vis absorbance and the fluorescence intensity. Compared to previous works, our biosensor shows following merits: Firstly, the antibody coated 96-well plate-based platform isolates exosomes via a simple and fast manner. Secondly, hydrophobic reaction-based membrane modification is spontaneous with high affinity, which induces a large amount of signal probes on the surface of exosomes that help amplify the signals. The LOD is as low as 3.40×10^3 particles μL^{-1} and 3.12×10^3 particles μL^{-1} for colorimetric and fluorescent methods, respectively. Thirdly, the colorimetric and complementary fluorescent signals enrich detection avenue. Lastly, this biosensor shows the capability to monitor the difference of exosomes concentration between serums from breast cancer patients and healthy individuals. Moreover, the performance of this biosensor is expected to be refined in the future. Continued research on employing multivalent antibody to act as recognition element, which is promising for improving the selectivity. At the same time, the relevant aptamer is expected to capture the exosomes in future work, improving the stability of this method. Consequently, we envision this designed biosensor will open up a new possibility for disease screening in exosomes detection.

CRediT authorship contribution statement

Yaokun Xia: Conceptualization, Writing - original draft. **Tingting Chen:** Validation, Writing - original draft. **Guanyu Chen:** Methodology, Investigation. **Yunping Weng:** Formal analysis, Visualization. **Lupeng Zeng:** Methodology. **Yijuan Liao:** Visualization, Formal analysis. **Wenqian Chen:** Data curation. **Jianming Lan:** Data curation. **Jing Zhang:** Writing - review & editing, Project administration, Funding acquisition. **Jinghua Chen:** Resources, Writing - review & editing, Funding acquisition, Supervision.

Table 1
Recovery results of exosomes spiked into 1% diluted FBS by this biosensor.

Add	Found by colorimetry	Recovery (%)	RSD (%)	Found by fluorescence	Recovery (%)	RSD (%)
0.5	0.48 ± 0.0093	96.0	1.92	0.42 ± 0.0038	84.0	0.90
1	0.99 ± 0.073	99.0	7.38	1.14 ± 0.061	114.0	4.33
2	2.02 ± 0.028	101.0	1.37	1.99 ± 0.17	99.5	3.47
3	3.31 ± 0.16	110.33	1.75	3.18 ± 0.21	106.0	4.10
4	4.09 ± 0.21	102.25	0.91	3.92 ± 0.15	98.0	2.66

Note: the concentration unit in above Table is 10^5 particles μL^{-1}.

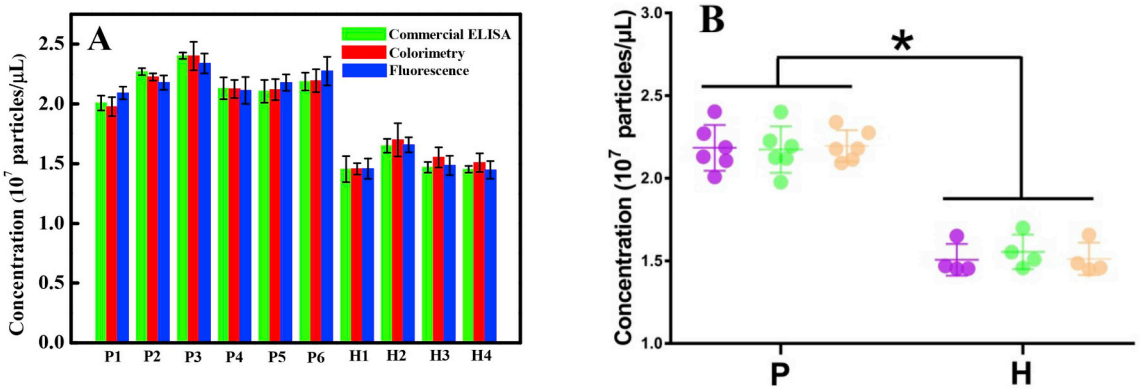

Fig. 5. (A) Comparison of this method and commercial ELISA kit for the detection of exosomes in real sample from six breast cancer patients (P) and four healthy donors (H). (B) Exosomes amount in serum of breast cancer patients (P, n = 6) and healthy donors (H, n = 4). Each symbol represents an individual subject. The purple symbols represent colorimetric method. The green symbols represent fluorescent method. The golden symbols represent ELISA. *P < 0.05 (two-tailed Student's t-test). (For interpretation of the references to color in this figure legend, the reader is referred to the Web version of this article.)

Acknowledgements

The authors gratefully acknowledge the financial support of National Natural Science Foundation of China (21874019), the Natural Science Foundation of Fujian Province (2017J07001), the United Fujian Provincial Health and Education Project for Tacking the Key Research P.R. China (WKJ2016-2-30), the Fujian Science and Technology Innovation Joint Found Project (2016Y9050), Startup Fund for Scientific Research, Fujian Medical University (2017XQ2015).

Appendix A. Supplementary data

Supplementary data to this article can be found online at https://doi.org/10.1016/j.talanta.2020.120851.

References

[1] P. Zhang, B. Dong, E. Zeng, F. Wang, Y. Jiang, D. Li, D. Liu, In vivo tracking of multiple tumor exosomes labeled by phospholipid-based bioorthogonal conjugation, Anal. Chem. 90 (2018) 11273–11279.
[2] K. Kalishwaralal, W.Y. Kwon, K.S. Park, Exosomes for non-invasive cancer monitoring, Biotechnol. J. 14 (2019) 1800430.
[3] B. Yang, Y. Chen, J. Shi, Exosome biochemistry and advanced nanotechnology for next-generation theranostic platforms, Adv. Mater. 31 (2019) 1802896.
[4] A.T. Jan, S. Rahman, S. Khan, S.A. Tasduq, I. Choi, Biology, pathophysiological role, and clinical implications of exosomes: a critical appraisal, Cells 8 (2019) 99.
[5] Y. Xia, L. Wang, J. Li, X. Chen, J. Lan, A. Yan, Y. Lei, S. Yang, H. Yang, J. Chen, A ratiometric fluorescent bioprobe based on carbon dots and acridone derivate for signal amplification detection exosomal microRNA, Anal. Chem. 90 (2018) 8969–8976.
[6] G. Qiu, A. Thakur, C. Xu, S.P. Ng, Y. Lee, C.M.L. Wu, Detection of glioma-derived exosomes with the biotinylated antibody-functionalized titanium nitride plasmonic biosensor, Adv. Funct. Mater. 29 (2019) 1806761.
[7] Y. Zhang, M. Yu, W. Tian, Physiological and pathological impact of exosomes of adipose tissue, Cell Prolif 49 (2016) 3–13.
[8] N. Wang, X. Song, L. Liu, L. Niu, X. Wang, X. Song, L. Xie, Circulating exosomes contain protein biomarkers of metastatic non-small-cell lung cancer, Canc. Sci. 109 (2018) 1701–1709.
[9] L. Tan, H. Wu, Y. Liu, M. Zhao, D. Li, Q. Lu, Recent advances of exosomes in immune modulation and autoimmune diseases, Autoimmunity 49 (2016) 357–365.
[10] T. Huang, C.X. Deng, Current progresses of exosomes as cancer diagnostic and prognostic biomarkers, Int. J. Biol. Sci. 15 (2019) 1–11.
[11] H. Shao, H. Im, C.M. Castro, X. Breakefield, R. Weissleder, H. Lee, New technologies for analysis of extracellular vesicles, Chem. Rev. 118 (2018) 1917–1950.
[12] C. Théry, K.W. Witwer, E. Aikawa, et al., Minimal information for studies of extracellular vesicles 2018 (MISEV2018): a position statement of the International Society for Extracellular Vesicles and update of the MISEV2014 guidelines, J. Extracell. Vesicles 7 (2018) 1–43.
[13] F. He, H. Liu, X. Guo, B.C. Yin, B.C. Ye, Direct exosome quantification via bivalent-cholesterol-labeled DNA anchor for signal amplification, Anal. Chem. 89 (2017) 12968–12975.
[14] Y. Xia, M. Liu, L. Wang, A. Yan, W. He, M. Chen, J. Lan, J. Xu, L. Guan, J. Chen, A visible and colorimetric aptasensor based on DNA-capped single-walled carbon nanotubes for detection of exosomes, Biosens. Bioelectron. 92 (2017) 8–15.
[15] Y.M. Wang, J.W. Liu, G.B. Adkins, W. Shen, M.P. Trinh, L.Y. Duan, J.H. Jiang, W. Zhong, Enhancement of the intrinsic peroxidase-like activity of graphitic carbon nitride nanosheets by ssDNAs and its application for detection of exosomes, Anal. Chem. 89 (2017) 12327–12333.
[16] Z. Zhang, C. Tang, L. Zhao, L. Xu, W. Zhou, Z. Dong, Y. Yang, Q. Xie, X. Fang, Aptamer-based fluorescence polarization assay for separation-free exosome quantification, Nanoscale 11 (2019) 10106–10113.
[17] L. Wang, Y. Yang, Y. Liu, L. Ning, Y. Xiang, G. Li, Bridging exosome and liposome through zirconium-phosphate coordination chemistry: a new method for exosome detection, Chem. Commun. 55 (2019) 2708–2711.
[18] Y. Lyu, D. Cui, J. Huang, W. Fan, Y. Miao, K. Pu, Near-infrared afterglow semiconducting nano-polycomplexes for the multiplex differentiation of cancer exosomes, Angew Chem. Int. Ed. Engl. 58 (2019) 4983–4987.
[19] M.L. Gao, F. He, B.C. Yin, B.C. Ye, A dual signal amplification method for exosome detection based on DNA dendrimer self-assembly, Analyst 144 (2019) 1995–2002.
[20] X. Chen, J. Lan, Y. Liu, L. Li, L. Yan, Y. Xia, F. Wu, C. Li, S. Li, J. Chen, A paper-supported aptasensor based on upconversion luminescence resonance energy transfer for the accessible determination of exosomes, Biosens. Bioelectron. 102 (2018) 582–588.
[21] D. Jin, F. Yang, Y. Zhang, L. Liu, Y. Zhou, F. Wang, G.J. Zhang, ExoAPP: exosome-oriented, aptamer nanoprobe-enabled surface proteins profiling and detection, Anal. Chem. 90 (2018) 14402–14411.
[22] N. Li, Z. Huang, Z. Ye, X. Zhang, L. Chen, Y. Xiao, Total membrane lipid assay (MLA): simple and practical quantification of exosomes based on efficient membrane-specific dyes unaffected by protein, Mater. Chem. Front. 2 (2018) 2130–2139.
[23] H. Wang, H. Chen, Z. Huang, T. Li, A. Deng, J. Kong, DNase I enzyme-aided fluorescence signal amplification based on graphene oxide-DNA aptamer interactions for colorectal cancer exosome detection, Talanta 184 (2018) 219–226.
[24] S. Wan, L. Zhang, S. Wang, Y. Liu, C. Wu, C. Cui, H. Sun, M. Shi, Y. Jiang, L. Li, L. Qiu, W. Tan, Molecular recognition-based DNA nanoassemblies on the surfaces of nanosized exosomes, J. Am. Chem. Soc. 139 (2017) 5289–5292.
[25] Y. Yang, E. Kannisto, G. Yu, M.E. Reid, S.K. Patnaik, Y. Wu, An immuno-biochip selectively captures tumor-derived exosomes and detects exosomal RNAs for cancer diagnosis, ACS Appl. Mater. Interfaces 10 (2018) 43375–43386.
[26] Q. Zhang, F. Wang, H. Zhang, Y. Zhang, M. Liu, Y. Liu, Universal Ti_3C_2 MXenes based self-standard ratiometric fluorescence resonance energy transfer platform for highly sensitive detection of exosomes, Anal. Chem. 90 (2018) 12737–12744.
[27] F. He, J. Wang, B.C. Yin, B.C. Ye, Quantification of exosome based on a copper-mediated signal amplification strategy, Anal. Chem. 90 (2018) 8072–8079.
[28] L. Huang, D.B. Wang, N. Singh, F. Yang, N. Gu, X.E. Zhang, A dual-signal amplification platform for sensitive fluorescence biosensing of leukemia-derived exosomes, Nanoscale 10 (2018) 20289–20295.
[29] A.A.I. Sina, R. Vaidyanathan, A. Wuethrich, L.G. Carrascosa, M. Trau, Label-free detection of exosomes using a surface plasmon resonance biosensor, Anal. Bioanal. Chem. 411 (2019) 1311–1318.
[30] D.L.M. Rupert, C. Lässer, M. Eldh, S. Block, V.P. Zhdanov, J.O. Lotvall, M. Bally, F. Höök, Determination of exosome concentration in solution using surface plasmon resonance spectroscopy, Anal. Chem. 86 (2014) 5929–5936.
[31] P. Zhang, X. Zhou, M. He, Y. Shang, A.L. Tetlow, A.K. Godwin, Y. Zeng, Ultrasensitive detection of circulating exosomes with a 3D-nanopatterned microfluidic chip, Nat. Biomed. Eng. 3 (2019) 438–451.
[32] H. Xu, C. Liao, P. Zuo, Z. Liu, B.C. Ye, Magnetic-based microfluidic device for on-chip isolation and detection of tumor-derived exosomes, Anal. Chem. 90 (2018) 13451–13458.
[33] E.A. Kwizera, R. O'Connor, V. Vinduska, M. Williams, E.R. Butch, S.E. Snyder, X. Chen, X. Huang, Molecular detection and analysis of exosomes using surface-enhanced Raman scattering gold nanorods and a miniaturized device, Theranostics 8 (2018) 2722–2738.
[34] Y.F. Tian, C.F. Ning, F. He, B.C. Yin, B.C. Ye, Highly sensitive detection of exosomes by SERS using gold nanostar@Raman reporter@nanoshell structures modified with

a bivalent cholesterol-labeled DNA anchor, Analyst 143 (2018) 4915–4922.
[35] T.D. Li, R. Zhang, H. Chen, Z.P. Huang, X. Ye, H. Wang, A.M. Deng, J.L. Kong, An ultrasensitive polydopamine bi-functionalized SERS immunoassay for exosome-based diagnosis and classification of pancreatic cancer, Chem. Sci. 9 (2018) 5372–5382.
[36] Z. Wang, S. Zong, Y. Wang, N. Li, L. Li, J. Lu, Z. Wang, B. Chen, Y. Cui, Screening and multiple detection of cancer exosomes using an SERS-based method, Nanoscale 10 (2018) 9053–9062.
[37] Y. Pang, C. Wang, L. Lu, C. Wang, Z. Sun, R. Xiao, Dual-SERS biosensor for one-step detection of microRNAs in exosome and residual plasma of blood samples for diagnosing pancreatic cancer, Biosens. Bioelectron. 130 (2019) 204–213.
[38] H. Zhang, Z. Wang, Q. Zhang, F. Wang, Y. Liu, Ti_3C_2 MXenes nanosheets catalyzed highly efficient electrogenerated chemiluminescence biosensor for the detection of exosomes, Biosens. Bioelectron. 124–125 (2019) 184–190.
[39] K. Boriachek, M.K. Masud, C. Palma, H.P. Phan, Y. Yamauchi, M.S.A. Hossain, N.T. Nguyen, C. Salomon, M.J.A. Shiddiky, Avoiding pre-Isolation step in exosome analysis: direct isolation and sensitive detection of exosomes using gold-loaded nanoporous ferric oxide nanozymes, Anal. Chem. 91 (2019) 3827–3834.
[40] R. Huang, L. He, Y. Xia, H. Xu, C. Liu, H. Xie, S. Wang, L. Peng, Y. Liu, Y. Liu, N. He, Z. Li, A sensitive aptasensor based on a Hemin/G-Quadruplex-assisted signal amplification strategy for electrochemical detection of gastric cancer exosomes, Small 15 (2019) 1900735.
[41] K. Boriachek, M.N. Islam, V. Gopalan, A.K. Lam, N.T. Nguyen, M.J.A. Shiddiky, Quantum dot-based sensitive detection of disease specific exosome in serum, Analyst 142 (2017) 2211–2219.
[42] H. Dong, H. Chen, J. Jiang, H. Zhang, C. Cai, Q. Shen, Highly sensitive electrochemical detection of tumor exosomes based on aptamer recognition-induced multi-DNA release and cyclic enzymatic amplification, Anal. Chem. 90 (2018) 4507–4513.
[43] S. Jeong, J. Park, D. Pathania, C.M. Castro, R. Weissleder, H. Lee, Integrated magneto-electrochemical sensor for exosome analysis, ACS Nano 10 (2016) 1802–1809.
[44] X. Doldán, P. Fagúndez, A. Cayota, J. Laíz, J.P. Tosar, Electrochemical sandwich immunosensor for determination of exosomes based on surface marker-mediated signal amplification, Anal. Chem. 88 (2016) 10466–10473.
[45] Y. Song, Y. Shi, M. Huang, W. Wang, Y. Wang, J. Cheng, Z. Lei, Z. Zhu, C. Yang, Bioinspired engineering of a multivalent aptamer-functionalized nanointerface to enhance the capture and release of circulating tumor cells, Angew. Chem. Int. Ed. 58 (2019) 2236–2240.
[46] C.Y. Tay, L. Yuan, D.T. Leong, Nature-inspired DNA nanosensor for real-time in situ detection of mRNA in living cells, ACS Nano 9 (2015) 5609–5617.
[47] Y. Lei, J. Tang, H. Shi, X. Ye, X. He, F. Xu, L. Yan, Z. Qiao, K. Wang, Nature-inspired smart DNA nanodoctor for activatable in vivo cancer imaging and in situ drug release based on recognition-triggered assembly of split aptamer, Anal. Chem. 88 (2016) 11699–11706.
[48] E.A. Alipanahpour Dil, A. Asfaram, F. Sadeghfar, Magnetic dispersive micro-solid phase extraction with the CuO/ZnO@Fe_3O_4-CNTs nanocomposite sorbent for the rapid pre-concentration of chlorogenic acid in the medical extract of plants, food, and water samples, Analyst 144 (2019) 2684–2695.
[49] E.A. Dil, M. Ghaedi, A. Asfaram, Application of hydrophobic deep eutectic solvent as the carrier for ferrofluid: a novel strategy for pre-concentration and determination of mefenamic acid in human urine samples by high performance liquid chromatography under experimental design optimization, Talanta 202 (2019) 526–530.
[50] Z. Moradi, E. Alipanahpour Dil, A. Asfaram, Dispersive micro-solid phase extraction based on Fe_3O_4@SiO_2@Ti-MOF as a magnetic nanocomposite sorbent for the trace analysis of caffeic acid in the medical extracts of plants and water samples prior to HPLC-UV analysis, Analyst 144 (2019) 4351–4361.
[51] E. Alipanahpour Dil, M. Ghaedi, A. Asfaram, F. Mehrabi, A.A. Bazrafshan, Optimization of process parameters for determination of trace Hazardous dyes from industrial wastewaters based on nanostructures materials under ultrasound energy, Ultrason. Sonochem. 40 (2018) 238–248.
[52] F. Mehrabi, A. Vafaei, M. Ghaedi, A.M. Ghaedi, E. Alipanahpour Dil, A. Asfaram, Ultrasound assisted extraction of Maxilon Red GRL dye from water samples using cobalt ferrite nanoparticles loaded on activated carbon as sorbent: optimization and modeling, Ultrason. Sonochem. 38 (2017) 672–680.
[53] T.F. Bruce, T.J. Slonecki, L. Wang, S. Huang, R.R. Powell, R.K. Marcus, Exosome isolation and purification via hydrophobic interaction chromatography using a polyester, capillary-channeled polymer fiber phase, Electrophoresis 40 (2019) 571–581.
[54] C.P. Lai, O. Mardini, M. Ericsson, S. Prabhakar, C.A. Maguire, J.W. Chen, B.A. Tannous, X.O. Breakefield, Dynamic biodistribution of extracellular vesicles in vivo using a multimodal imaging reporter, ACS Nano 8 (2014) 483–494.
[55] Y. Wan, G. Cheng, X. Liu, S.J. Hao, M. Nisic, C.D. Zhu, Y.Q. Xia, W.Q. Li, Z.G. Wang, W.L. Zhang, S.J. Rice, A. Sebastian, I. Albert, C.P. Belani, S.Y. Zheng, Rapid magnetic isolation of extracellular vesicles via lipid-based nanoprobes, Nat. Biomed. Eng. 1 (2017) 0058.
[56] H. Etayash, A.R. McGee, K. Kaur, T. Thundat, Nanomechanical sandwich assay for multiple cancer biomarkers in breast cancer cell-derived exosomes, Nanoscale 8 (2016) 15137–15141.
[57] J. Sun, J. Zhao, L. Wang, H. Li, F. Yang, X. Yang, Inner filter effect-based sensor for horseradish peroxidase and its application to fluorescence immunoassay, ACS Sens. 3 (2018) 183–190.
[58] B. Liu, J. Liu, Freezing directed construction of bio/nano interfaces: reagentless conjugation, denser spherical nucleic acids, and better nanoflares, J. Am. Chem. Soc. 139 (2017) 9471–9474.
[59] S.Q. Chai, W.Y. Lv, J.H. He, C.H. Li, Y.F. Li, C.M. Li, C.Z. Huang, Dual energy transfer-based fluorescent nanoprobe for imaging miR-21 in nonalcoholic fatty liver cells with low background, Anal. Chem. 91 (2019) 6761–6768.
[60] H.C. Chang, J.A. Ho, Gold nanocluster-assisted fluorescent detection for hydrogen peroxide and cholesterol based on the inner filter effect of gold nanoparticles, Anal. Chem. 87 (2015) 10362–10367.
[61] H. Chen, Q. Lu, K. He, M. Liu, Y. Zhang, S. Yao, A cyclic signal amplification strategy to fluorescence and colorimetric dual-readout assay for the detection of H_2O_2-related analytes and application to colorimetric logic gate, Sensor. Actuator. B Chem. 260 (2018) 908–917.
[62] R.H. Wang, C.L. Zhu, L.L. Wang, L.Z. Xu, W.L. Wang, C. Yang, Y. Zhang, Dual-modal aptasensor for the detection of isocarbophos in vegetables, Talanta (2019), https://doi.org/10.1016/j.talanta.2019.06.094.
[63] M. You, Y. Lyu, D. Han, L. Qiu, Q. Liu, T. Chen, C. Sam Wu, L. Peng, L. Zhang, G. Bao, W. Tan, DNA probes for monitoring dynamic and transient molecular encounters on live cell membranes, Nat. Nanotechnol. 12 (2017) 453–459.
[64] W. Zhang, P. Peng, Y. Kuang, J. Yang, D. Cao, Y. You, K. Shen, Characterization of exosomes derived from ovarian cancer cells and normal ovarian epithelial cells by nanoparticle tracking analysis, Tumor Biol. 37 (2016) 4213–4221.
[65] B. Qiao, Q. Guo, J. Jiang, Y. Qi, H. Zhang, B. He, C. Cai, J. Shen, An electrochemiluminescent aptasensor for amplified detection of exosomes from breast tumor cells (MCF-7 cells) based on G-quadruplex/hemin DNAzymes, Analyst 144 (2019) 3668–3675.
[66] Y. Wang, D. Luo, Y. Fang, W. Wu, Y. Wang, Y. Xia, F. Wu, C. Li, J. Lan, J. Chen, An aptasensor based on upconversion nanoparticles as LRET donors for the detection of exosomes, Sensor. Actuator. B Chem. (2019), https://doi.org/10.1016/j.snb.2019.126900.
[67] V. Gonzalez-Villasana, M.H. Rashed, Y. Gonzalez-Cantú, R. Bayraktar, J.L. Menchaca-Arredondo, J.M. Vazquez-Guillen, C. Rodriguez-Padilla, G. Lopez-Berestein, D. Resendez-Perez, Presence of circulating miR-145, miR-155, and miR-382 in exosomes isolated from serum of breast cancer patients and healthy donors, Dis. Markers 2019 (2019) 6852917.
[68] M. Wu, Y. Ouyang, Z. Wang, R. Zhang, P.H. Huang, C. Chen, H. Li, P. Li, D. Quinn, M. Dao, S. Suresh, Y. Sadovsky, T.J. Huang, Isolation of exosomes from whole blood by integrating acoustics and microfluidics, Proc. Natl. Acad. Sci. U. S. A. 114 (2017) 10584–10589.
[69] S.A. Melo, L.B. Luecke, C. Kahlert, A.F. Fernandez, S.T. Gammon, J. Kaye, V.S. LeBleu, E.A. Mittendorf, J. Weitz, N. Rahbari, C. Reissfelder, C. Pilarsky, M.F. Fraga, D. Piwnica-Worms, R. Kalluri, Glypican-1 identifies cancer exosomes and detects early pancreatic cancer, Nature 523 (2015) 177–182.